IJIE

UTHM Penerbit

INTERNATIONAL JOURNAL OF INTEGRATED ENGINEERING
ISSN: 2229-838X e-ISSN: 2600-7916

Vol. 18 No. 3 (2026) 177-197
https://publisher.uthm.edu.my/ojs/index.php/ijie

Structural Health Monitoring of Marine Propellers Using Strain Modal Parameters

Rachid Azzi[1,2]*, Farid Asma[1]

[1] *Laboratory of Elaboration, Characterization of Materials and Modelling, Mouloud Mammeri University, Tizi Ouzou, BP 17 RP 15000, ALGERIA*

[2] *Department of Mechanical Engineering, University M'Hamed Bougara of Boumerdes, Independence Avenue, Boumerdes, 35000, ALGERIA*

*Corresponding Author: r.azzi@univ-boumerdes.dz
DOI: https://doi.org/10.30880/ijie.2026.18.03.012

Article Info

Received: 9 June 2025
Accepted: 7 December 2025
Available online: 25 May 2026

Keywords

Marine propeller blade, damage identification, strain modal parameters

Abstract

The marine propeller in operation undergoes local defects on the surface and edges of the blades, thus causing vibrations of the propulsion system and a reduction of the propulsion efficiency of the propeller. These local defects develop gradually under the effect of cyclic stresses and lead to the failure of the marine propeller blade by fatigue. In this article, a unique non-destructive approach for structural defect identification in marine propeller blades is presented. The defect identification methods defined by modal strains, such as strain mode shapes changes, strain flexibility changes, and defect index, were used to find and identify single and multiple defects in the marine propeller blade's structure. The modal strain-related defect indicators were calculated from the strain mode shapes. The strain mode shapes of the marine propeller blade are tri-axial and are calculated along the x, y, and z directions of vibration. In this article, three defect types were considered, with different sizes along the length of the three guide curves starting from the blade base to the free end. The results proved that the proposed defect identification methods defined by modal strains can accurately locate single and multiple defects up to four appearing on the leading edge, the trailing edge, and the propeller blade surface. The magnitude of the defect index at nodes of defective elements is higher (order of 10^{-2}) than the magnitude of strain mode shapes change (order of 10^{-3}), and much higher than the magnitude of strain flexibility change, which is of the order of 10^{-9}. The defect severity quantification on a marine propeller blade is feasible as the magnitudes of the three proposed defect indicators at the nodes of the defective elements are proportional to the severity of the defects.

1. Introduction

In the maritime industry, the marine propeller is one of the most vital and expensive elements of a ship's propulsion system. It used to move the ship through the water. The propeller incorporates radially arranged blades around the hub with equal angular spacing. The rotation of the propeller blades produces thrust by driving the surrounding water backward, propelling the ship forward. However, marine propeller blades, after a short or long period of operation, have been suffering from local defects of different origins. Marine propellers are obtained by different casting methods; they contain damages inherited from this manufacturing process (pores, nonmetallic inclusions, surface flaws, etc.) that contribute to crack initiation and reduction of fatigue strength. In the service, marine propeller blades are subject to cyclic loading and are exposed to a hostile environment, corrosion, abrasion, impact with foreign objects, etc. [1]. Several cases of propeller blade failures have been reported in the maritime service [2], [3]. In recent years, several studies on the failure analysis of marine propellers have appeared, in which the purpose is to determine the causes of the failure of the blades and to propose corrective actions to minimize this problem [4]. Some other related studies focus on the fatigue life of propeller materials [5], [6]. The damages inherited from the casting process, environmental conditions, and improper user maneuvers all contribute to the initiation of cracks on the blade circumference and their propagation under low stress.

The marine propeller undergoes the final product quality system by nondestructive testing, such as penetrant testing for detection of surface flaws, and during service, is inspected for possible structural damage and cracks. However, small damage and cracks on the marine propeller in operation accumulate salt deposits and close, which makes their detection by traditional methods, non-destructive testing, extremely difficult. The appearance of a crack or any other structural damage on the propeller blade is a very serious situation that systematically leads to the rupture of the blade and the stopping of boat navigation, which can only be restored by propeller replacement. Therefore, it becomes imperative to identify structural defects in the propeller blade structure as soon as possible. Precocious defect detection enables scheduled repair by grinding or welding carried out by a propeller specialist at a relatively low cost, which extends the life of the entire propeller.

Dynamic strain-related defect identification methods have attracted much attention and are promising alternative to non –destructive testing methods in structural health monitoring; they are very sensitive to light structural defects [7], [8], and in practical applications with noisy conditions, they can unambiguously detect and locate unique and many defects in the structures [9]. The research on the application of vibration-based damage detection methods to the marine propeller blades is limited. Some related research works, including strain modal analysis of propeller blades, and the current methods based on modal displacement/strain parameters to local defects in real structures, are reviewed in the following. As for the modal strain parameters calculation of marine propeller blades, Huang Zheng et al. [10] have compared the modal properties of the composite propeller blade with those of the metal propeller using the finite element method and experimental strain modal analysis. They demonstrated that the natural frequencies of the composite propeller are smaller compared to those of the metal propeller, and its structural damping is higher than that of the metal propeller. On the other hand, the strain mode shapes of the two propellers are similar. Y. Hong et al. [11] have investigated the dynamic response of two ship's propeller blades, one rigid and another composite. They concluded that the modal characteristics of the composite blade are different from those of the rigid blade, and the influence of added mass is significant for the composite blade than for the metal blade. Saeed Javdani et al. [12] investigated experimentally the vibration behavior of marine propeller blades in dry and wet conditions. The authors confirmed that the natural frequencies of the propeller blade in water are lower than those in air, and the modes of vibration in air and water are the same. H.J. Lin and J.F. Tsai [13] analyzed the modal characteristics of metal and composite propeller blades in air and water. They concluded that the submersion of the blade in the water causes a significant reduction in natural frequencies with a high percentage for composite blades, and the mode shapes of the two types of blades remain the same in air and water. In all these studies, the dynamic strains and displacements in the x, y, and z directions were not considered; only the resultant components of these parameters were analyzed.

Displacement/strain modal parameter-based damage diagnostics methods have emerged as powerful for damage detection and identification in rotating blades. Recently, R. Azzi and F. Asma [14] published research on detecting impact defects on the edge of the marine propeller blade under operating conditions by comparing the modal parameters and the time response of the intact blade to those of the damaged blade. Dos Santos et al. [15] applied the compatibility of mode forms and the modal strain energy method to damage identification in composite helicopter rotor blades using the experimental results from the modal analysis. Zefeng Wang et al. [16] have compared the undamaged and damaged strain modes of composite rotor blades and have concluded that damage localization based on strain modes is feasible. An experimental study was conducted by Ming Zhang et al. [17] to examine the dynamic behavior of the Kaplan turbine blade both before and after the emergence of a crack. The results found show that the natural frequency values of the blade decrease for all vibration modes when there is a crack. The modal displacements do not vary much with the presence of the crack, but the modal stress distribution changes significantly for all examined modes. Yanfeng Wang et al. [18] applied two techniques, the difference in modal displacement and the difference in curvature of modal displacement, for localizing single and multiple defects in a 3D model of wind turbine blades. The authors showed that the mode shape difference obtained at measurement points is a 3D surface. So, the spatial position of damages is indicated by the large value of the difference in modal displacement and by the maximal or minimal curvature value of the surface formed by the difference between the modal displacements of the blade without defect and those of the blade with defect. Mohamed M. Rezaei et al. [19] investigated a group of damage indicators defined by the modal parameters such as natural frequency, displacement mode, curvature of displacement mode, modal assurance criterion, and modal strain energy in the modern wind turbine blade. K. Tatsis et al. [20] have done a numerical study on small-scale models of wind turbine blades subjected to some possible damage cases under both environmental (temperature) and operational (rotation velocity) variability. The frequencies, transmissibility functions, and mode shape curvature have been used for detecting and localizing structural defects. Wasanthi R. Wickramasinghe et al. [21], [22] adapted the defect index defined by the modal flexibility by considering the vertical and lateral components of the mode form for detecting and localizing single or multiple defect scenarios in a bridge with a pre-tensioned cable. Huajun Li et al. [23] proposed to decompose the defect index defined by the modal strain energy of each of the 3D structure elements into two defect indices, axial and transverse. The prior vibration–based defect identification techniques utilized the resultant components of the strain/displacement mode shapes or the lateral and vertical components of mode shapes to calculate the defect indices.

The geometry of the marine propeller blade is complex. Therefore, the vibration mode shapes of propeller blades are tri-axial and often have components in the three axes of vibration, x, y, and z. Following that, the mode shapes must be expressed in the x, y, and z directions. All of the mode-shape components appear to be important. Therefore, it is useful to express the defect indicators depending on the three mode shape components. In this article, the conventional strain-related identification damage indices are accommodated to the three strain mode components. One defect indicator uses the x-component of the strain mode form, the second defect indicator uses the y-component of the strain mode form, and the third defect indicator uses the z-component of the strain mode form. Strain-based damage indicators built in the three directions of vibrations have not been treated in the literature. This article proposes a collection of techniques for detecting and identifying structural damage in marine propeller blades. These techniques are defined by the strain modes shapes in x, y, and z directions, determined via the strain modal analysis. These methods can detect, locate, and assess the gravity of unique and multiple defects in marine propeller blades. To our knowledge, these methods for detecting defects in marine propeller blades have not been treated in the literature.

2. Marine Propeller Blade Model

The marine propeller blade model used in this study has been developed using the OpenProp code [24] and SolidWorks CAD software. The 3-D solid model of the marine propeller blade is illustrated in Fig. 1. The main geometrical properties of propellers are given in Table 1. The meshing of the model of the propeller blade was realized using the Ansys program, as illustrated in Fig. 2, which is then used to do the strain modal analysis. The two edges of the propeller blade, namely the leading edge and the trailing edge, are divided into 100 divisions. Both sections of the blade root and blade tip are divided into 40 divisions, respectively.

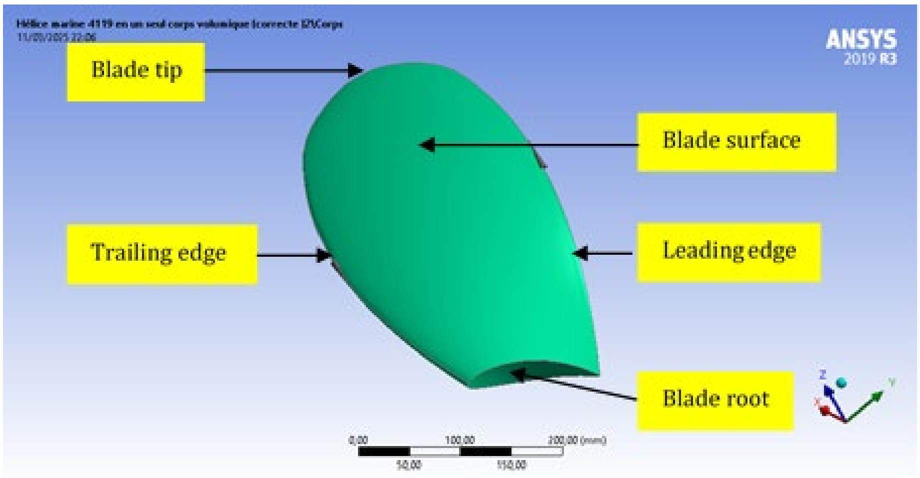

Fig. 1 *3D solid model of a marine propeller blade*

Table 1 *Geometrical characteristics of propeller blade*

Description	Capacity
Propeller Diameter	1 m
Number of Blades	3
Propeller Speed	72 RPM
Propeller Hub Diameter	0.2 m
Mean line Type	NACA a=0.8
Thickness Type	NACA 66

The propeller blade structure was meshed with a hexahedral mesh using the multi-zone method. The fully discretized model of the propeller blade contained 20347 nodes and 3800 elements. The material of the propeller blade is 2014-T4 aluminum [10], and its characteristics are a density of 2800 kg/m^3, Young's modulus E=75000 MPa, and Poisson's ratio μ=0.33. The propeller blade is fixed at the root using a fixed support.

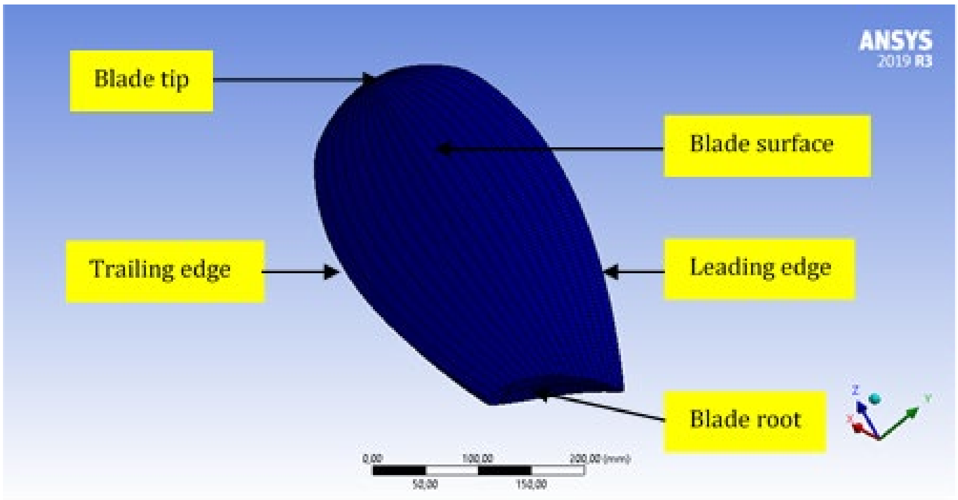

Fig. 2 *Meshing of the marine propeller blade*

3. Simulated Damage Configuration and Measurement Points

According to the probable damage appearance sites on the marine propeller blade, three structural damage types were considered: damage on the trailing edge, damage on the blade surface, and damage on the leading edge, as shown in Figs. 3-5. The first configuration represents damage on the trailing edge (see Fig. 3). In this damage type, the damaged element takes two radial positions along the trailing edge from the base to the free end of the blade, finite element numbers 3006 and 3168, as shown in Figure 3. For this damage type, the first three strain modal forms of the propeller blade were calculated in the x, y, and z directions along the 101 selected nodes of the trailing edge line, starting from the base to the free end of the propeller blade. The second damage type is damage to the blade pressure surface (see Fig. 4). The specified damaged element numbers are 1630 and 2920. For this damage type, the first three strain mode forms of the marine propeller blade were calculated in the x, y, and z directions and along the 101 selected nodes of the guide curve starting from the blade base to the free end, as shown in Fig. 4. Structural damage to the propeller blade's leading edge is the other kind of damage. As seen in Fig. 5, the damaged element for this damage type occupies four locations along the leading edge: finite element numbers 3213, 3351, 3465, and 3069. For damage type on the leading edge, the strain modal forms of the propeller blade were calculated in the x, y, and z directions and along the 101 nodes of the leading edge line, numbered from the blade base to the free end. The different defect cases inserted in the propeller blade and examined in this article are summarized in Table 2.

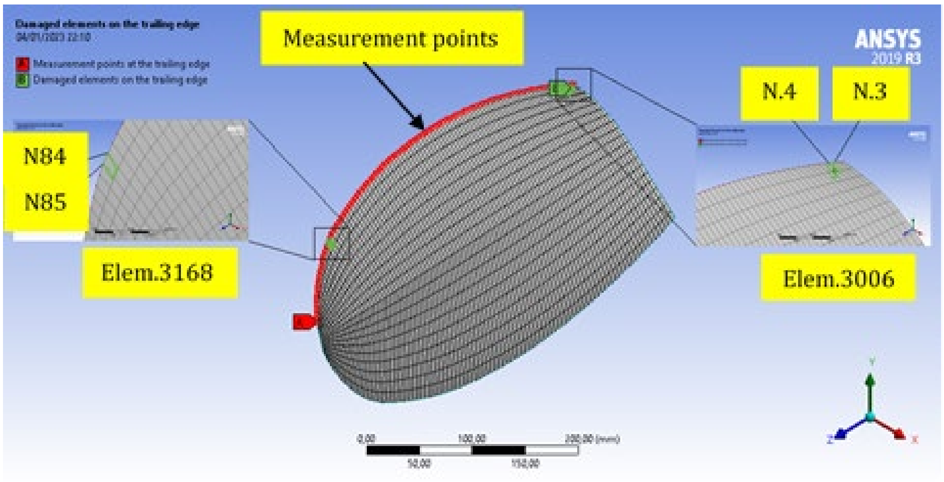

Fig. 3 *FE model of a propeller blade with damaged elements on the trailing edge and the measurement points*

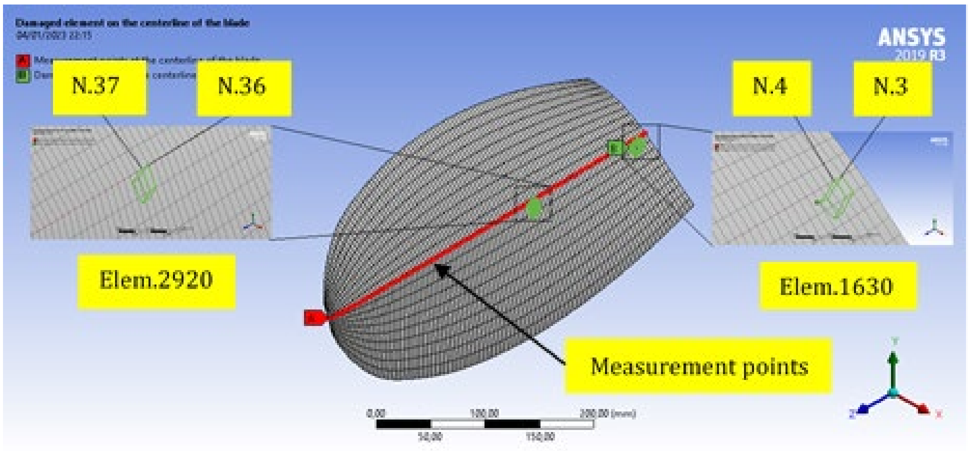

Fig. 4 *FE model of a propeller blade with damaged elements on the surface of the propeller blade and the measurement points*

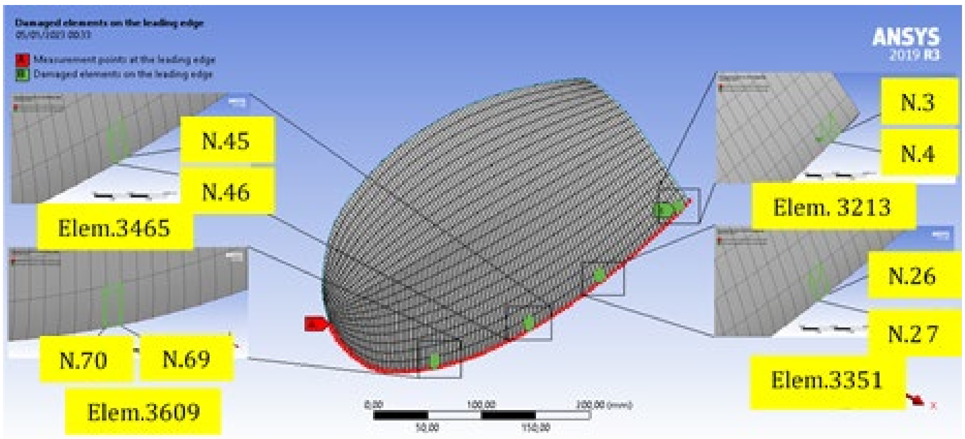

Fig. 5 *FE model of a propeller blade with damaged elements on the leading edge of the blade and the measurement points*

The damage is then inserted in the model of the marine propeller blade as a diminution in the mechanical properties (elasticity modulus) of a single specified finite element or several specified finite elements for multiple damage cases. The damage size varies from a light degree (10% reduction of elasticity modulus) to a severe degree (50%) with a step of 20%. The elasticity modulus of the damaged element is expressed as:

$$E_{damaged} = (1-\alpha)E_{undamaged} \tag{1}$$

Where α express the damage severity and takes successively three levels: 0.1 (10% for light damage), 0.3 (30% for moderate damage), and 0.5 (50% for severe damage).

4. Strain Modal Analysis of Damaged and Undamaged Propeller Blades

The forced vibration equation of a mechanical system of N degrees of freedom can be expressed as [17]:

$$[M]\{\ddot{x}(t)\} + [C]\{\dot{x}(t)\} + [K]\{x(t)\} = \{f(t)\} \tag{2}$$

Where $[M]$, $[C]$ and $[K]$ are, respectively, the mass, damping, and stiffness matrices. $\{f(t)\}$ is a force vector in the time domain. $\{x(t)\}$, $\{\dot{x}(t)\}$ and $\{\ddot{x}(t)\}$ are, respectively, the displacement, velocity, and acceleration vectors in the N points of the mechanical system in the time domain. For an undamped free mechanical system, equation (2) can be rewritten as [8]:

$$([K]-\omega^2[M])\Phi = 0 \tag{3}$$

The natural frequencies $\omega = [\omega_1, \omega_2, ..., \omega_n]$, and displacement mode shape $\Phi = [\phi_1, \phi_2, ..., \phi_n]$ can be determined from equation (3). The strain modal forms $\Psi = [\varphi_1^\varepsilon, \varphi_2^\varepsilon, ..., \varphi_n^\varepsilon]$ can be obtained from the relationship between the i^{th} strain modal φ_i^ε and the i^{th} displacement modal ϕ_i as [25]:

$$\varphi_i^\varepsilon = \theta\phi_i \tag{4}$$

Where θ is a matrix that varies with the structural geometry and boundary conditions.

Table 2 *The different damage scenarios in the marine propeller blade*

Damage type	Damage case	Damaged element number	Selected nodes of the damaged element
Single damage on the trailing edge	1	3006	(3, 4)
	2	3168	(84, 85)
Single damage in the blade surface	3	1630	(3, 4)
	4	2920	(36, 37)
Multiple damages on the leading edge	5	3213, 3351	(3,4), (27,28)
	6	3213, 3351, 3465	(3,4), (26,27), (45,46)
	7	3213,3351,3465,3609	(3,4), (27,28), (45,46), (69,70)

Finite element analysis software was used in this article to conduct the strain modal analysis of a marine propeller blade, and the i^{th} strain modal form is considered as the strain state of the marine propeller blade when it vibrates at the i^{th} natural frequency. In this article, the first three-strain modal forms in the tri-axial axis are calculated for the undamaged case and each damaged case of the marine propeller blade. The first three strain modal forms in the three directions are plotted to visualize the modal strain distribution, obviously of the intact model of the marine propeller blade, as illustrated in Fig. 6. From the strain distribution on the overall model of the marine propeller blade, the site of higher values of the modal strain changes from one mode to another. For each mode, the site of the higher values of the modal strain is not the same in the x, y, and z directions.

The strain mode forms have three components according to the vibration axis x, y, and z. The modal strain distribution according to the three axes is very different. Figure 7 shows the maximum amplitude of the modal strain components for the first three vibration modes on the trailing edge, on the blade surface, and on the leading edge. For all vibration modes considered, the z-component of the modal strain is higher than the other components for the different places of the propeller blade. On the leading and trailing edges, the z-component of the strain mode forms increases as the order of the mode increases. On the blade surface, the z-component of the strain mode is higher for the second order.

5. Modal Strain-Related Defect Identification Techniques

In this section, various strain-related damage identification techniques, such as strain mode shape change, strain flexibility change, and damage index, are presented in the x, y, and z directions for the case where several vibration modes of the structure were considered.

5.1 Strain Modal Change

The strain mode form displays the strain distribution state of the structure when vibrated at frequency ω_i. A. S.J. Swamidas and Y. Chen [26] applied the normalized strain mode forms change to locate the defect on the cantilever plate. In this article, the strain mode forms were calculated only along the three guide curves starting from the blade root to the blade tip and in three directions: x, y, and z. The defect index defined by the change in strain mode shapes called Strain Mode Shape Change (SMSC) is adapted for the three directions of vibration and given by:

$$(SMSC)_x = \frac{1}{n}\sum_{i=1}^{n}\left|\left((\varphi_{ij}^{\varepsilon})_x\right)_D - \left((\varphi_{ij}^{\varepsilon})_x\right)_H\right| \quad (5)$$

$$(SMSC)_y = \frac{1}{n}\sum_{i=1}^{n}\left|\left((\varphi_{ij}^{\varepsilon})_y\right)_D - \left((\varphi_{ij}^{\varepsilon})_y\right)_H\right| \quad (6)$$

$$(SMSC)_z = \frac{1}{n}\sum_{i=1}^{n}\left|\left((\varphi_{ij}^{\varepsilon})_z\right)_D - \left((\varphi_{ij}^{\varepsilon})_z\right)_H\right| \quad (7)$$

Where, $(\varphi_{ij}^{\varepsilon})_x$, $(\varphi_{ij}^{\varepsilon})_y$, and $(\varphi_{ij}^{\varepsilon})_z$ are the values of the i^{th} strain mode form at the j^{th} node along the length of the guide curve starting from the blade base to the free end of the blade in the x, y, and z directions, respectively. The indices H and D indicate the states of the propeller blade before and after the defect's appearance, respectively. Where n is the number of considered modes. The points at which the SMSC takes its maximum value indicate the location of the defective element.

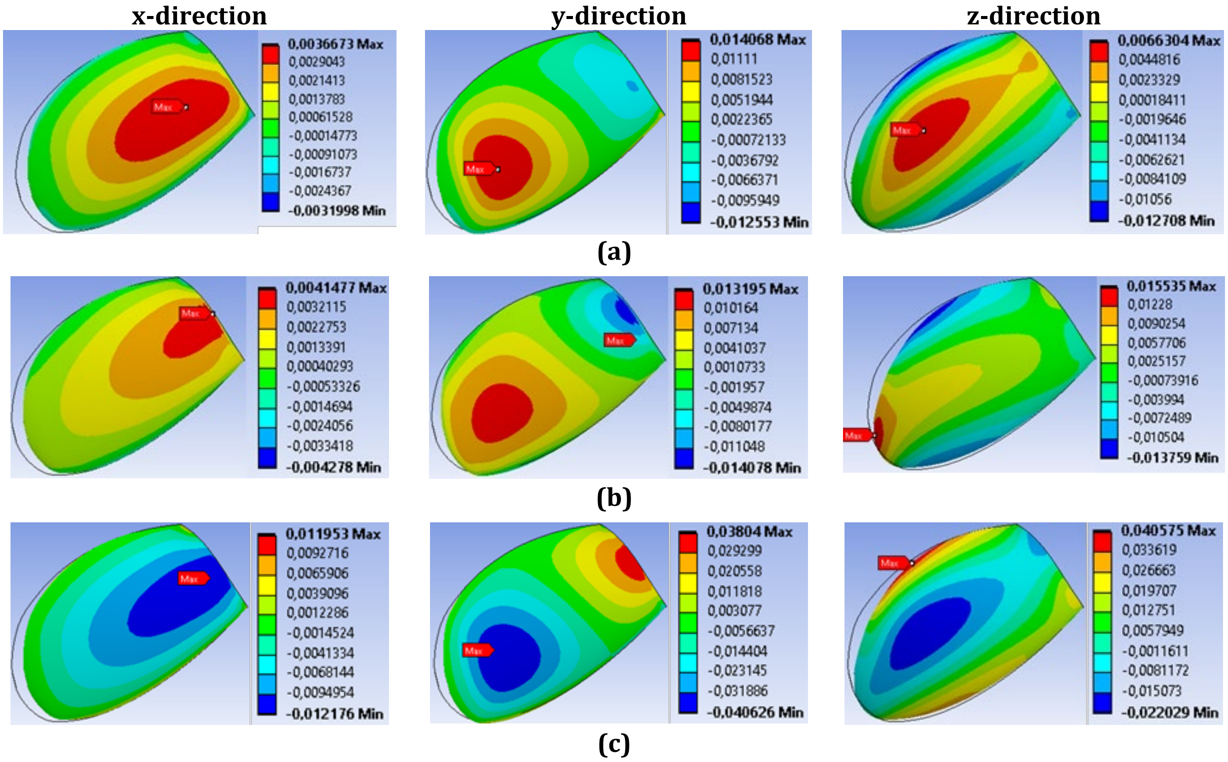

Fig. 6 *The first three-strain modal forms of an intact marine propeller blade in the x, y, and z directions. (a) First vibration mode; (b) Second vibration mode; (c) Third vibration mode*

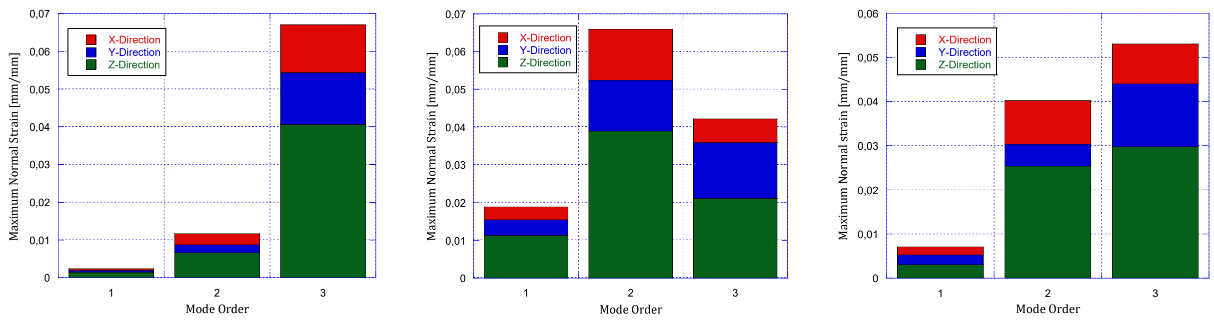

(a) **(b)** **(c)**

Fig. 7 *Maximum amplitude of the first three-strain mode forms in the x, y, and z-directions. (a) Modal strains on the trailing edge; (b) Modal strains on the blade surface; (c) Modal strains on the leading edge*

5.2 Strain Flexibility Change

Since strain modes are very influenced by the structural defect. Zonta et al. [27] have proposed the Strain Flexibility Change (SFC) damage detection method for damage assessment in steel bridges. M. Montazer and S. M. Seyedpoor [28] have proposed the SFC to locate multiple damages in truss systems. The method provides higher effectiveness in identifying multiple defects in the truss system and practical conditions. In the expression of SFC, the strain mode forms are used instead of the displacement mode forms. Since strain mode shapes were calculated in the three vibration directions x, y, and z. Then, the strain flexibility has three components as well and is computed using the strain mode shape components in x, y, and z. The change in strain flexibility $(SFC_j)_{x,y,z}$ in x, y, and z directions at a j[th] point of the structure is given by:

$$(SFC_j)_x = [(F_j^\varepsilon)_x]_D - [(F_j^\varepsilon)_x]_H = \left[\sum_{i=1}^{n}\frac{1}{\omega_i^2}\left(\varphi_{ij}^\varepsilon\right)_x\left(\varphi_{ij}^\varepsilon\right)_x^T\right]_D - \left[\sum_{i=1}^{n}\frac{1}{\omega_i^2}\left(\varphi_{ij}^\varepsilon\right)_x\left(\varphi_{ij}^\varepsilon\right)_x^T\right]_H \quad (8)$$

$$(SFC_j)_y = [(F_j^\varepsilon)_y]_D - [(F_j^\varepsilon)_y]_H = \left[\sum_{i=1}^{n}\frac{1}{\omega_i^2}\left(\varphi_{ij}^\varepsilon\right)_y\left(\varphi_{ij}^\varepsilon\right)_y^T\right]_D - \left[\sum_{i=1}^{n}\frac{1}{\omega_i^2}\left(\varphi_{ij}^\varepsilon\right)_y\left(\varphi_{ij}^\varepsilon\right)_y^T\right]_H \quad (9)$$

$$(SFC_j)_z = [(F_j^\varepsilon)_z]_D - [(F_j^\varepsilon)_z]_H = \left[\sum_{i=1}^{n}\frac{1}{\omega_i^2}\left(\varphi_{ij}^\varepsilon\right)_z\left(\varphi_{ij}^\varepsilon\right)_z^T\right]_D - \left[\sum_{i=1}^{n}\frac{1}{\omega_i^2}\left(\varphi_{ij}^\varepsilon\right)_z\left(\varphi_{ij}^\varepsilon\right)_z^T\right]_H \quad (10)$$

Where $(F_j^\varepsilon)_x$, $(F_j^\varepsilon)_y$, and $(F_j^\varepsilon)_z$ are the strain flexibility at the j[th] point of the structure in the x, y, and z directions, respectively. The points at which SFC achieves its maximum indicate the nodes of the defective element.

5.3 Defect Index

A Defect Index (DI) is a function of curvature mode forms and is formulated by the modal strain energy as developed in the reference [29]. Differentiating the displacement mode shapes provides the curvature mode shapes. Noise amplification is made possible by numerical differentiation, which lowers the damage index performance. The curvatures of mode shapes in a beam-like structure are strain mode shapes. In this article, the damage index formulation used is the one given by A. P. Adewuyi et al. [9], and instead of the second derivative of the displacement mode shape, the corresponding strain mode forms were used, as shown in the following equations.

In this article, the damage index $(DI_j)_{x,y,z}$ at the j[th] point of the structure is also calculated in the three directions using the components of strain mode shapes in the x, y, and z directions, as shown in equations (11), (12), and (13).

$$(DI_j)_x = \sum_{i=1}^{n} \frac{\left([(\varphi_{ij}^{\varepsilon})_x^2]_D + \sum_{j=1}^{N_0}[(\varphi_{ij}^{\varepsilon})_x^2]_D\right)\sum_{j=1}^{N_0}[(\varphi_{ij}^{\varepsilon})_x^2]_H}{\left([(\varphi_{ij}^{\varepsilon})_x^2]_H + \sum_{j=1}^{N_0}[(\varphi_{ij}^{\varepsilon})_x^2]_H\right)\sum_{j=1}^{N_0}[(\varphi_{ij}^{\varepsilon})_x^2]_D} - n \tag{11}$$

$$(DI_j)_y = \sum_{i=1}^{n} \frac{\left([(\varphi_{ij}^{\varepsilon})_y^2]_D + \sum_{j=1}^{N_0}[(\varphi_{ij}^{\varepsilon})_y^2]_D\right)\sum_{j=1}^{N_0}[(\varphi_{ij}^{\varepsilon})_y^2]_H}{\left([(\varphi_{ij}^{\varepsilon})_y^2]_H + \sum_{j=1}^{N_0}[(\varphi_{ij}^{\varepsilon})_y^2]_H\right)\sum_{j=1}^{N_0}[(\varphi_{ij}^{\varepsilon})_y^2]_D} - n \tag{12}$$

$$(DI_j)_z = \sum_{i=1}^{n} \frac{\left([(\varphi_{ij}^{\varepsilon})_z^2]_D + \sum_{j=1}^{N_0}[(\varphi_{ij}^{\varepsilon})_z^2]_D\right)\sum_{j=1}^{N_0}[(\varphi_{ij}^{\varepsilon})_z^2]_H}{\left([(\varphi_{ij}^{\varepsilon})_z^2]_H + \sum_{j=1}^{N_0}[(\varphi_{ij}^{\varepsilon})_z^2]_H\right)\sum_{j=1}^{N_0}[(\varphi_{ij}^{\varepsilon})_z^2]_D} - n \tag{13}$$

Where N_0 is the number of measurement points. The defective element is located between the points at which the $(DI)_{x, y, z}$ achieves its maximum.

6. Results and Discussion

Defect localization results for each defect case considered in Table 2 are presented below. As the z-component of modal strains is more important than other components, only the plots of defect indices in the *z*-direction along the length of the guide curves according to damage type are presented. The results are presented in three levels of damage sizes.

6.1 Single Damage Localization on the Trailing Edge of the Marine Propeller Blade

In this section, two defect cases were considered (damage case 1 and 2) to test the ability of the different strain-based identification methods to locate the single defective element along the trailing edge of the marine propeller blade. The damaged element numbers are 3006 and 3168, respectively. The defective element 3006 is near the blade tip, and the defective element 3168 is near the blade tip. On the numerical model of the propeller blade, two nodes of the defective finite element 3006 are situated at the 3rd and 4th points of the trailing edge from the blade base to the free end of the blade, and two nodes of the defective element 3168 are situated on the 88th and 89th points of the trailing edge. The first, second, and third strain mode forms in the *z*-direction are calculated along the 101 points (nodes) of the trailing edge for the healthy and defective models of the propeller blades. Then, the strain-based damage indicators, SMSC, SFC, and DI, were calculated in the z-direction using the first three strain mode forms and plotted along the trailing edge. The results of single damage localization on the trailing edge by SMSC, SFC, and DI are presented in the following sub-sections for varying damage severities, 10%, 30%, and 50%.

6.1.1 Strain Mode Shape Change-based Damage Indicator

Based on the z-component of the strain modal form, the strain mode shape changes $(SMSC)_z$ were computed in the z-direction using equation (7). The defect localisation results by the $(SMSC)_z$ for defect case 1 are shown in Fig. 8. The graph of SMSC along the trailing edge presents a peak; this indicates the presence of damage on the trailing edge. Damage case 1 consists of a specified damaged element 3006, which is at the third and fourth nodes of the trailing edge. It can be seen that the $(SMSC)_z$ attains its maximum at the predetermined nodes (3, 4) of the defective element for the various degrees of defect gravity, and then the $(SMSC)_z$ accurately locates the damaged element situated on the trailing edge and near the blade root. On the other hand, it can be observed that this feature can be utilized to measure the degree of damage intensity since the amplitude of the peak increases as the degree of damage severity increases.

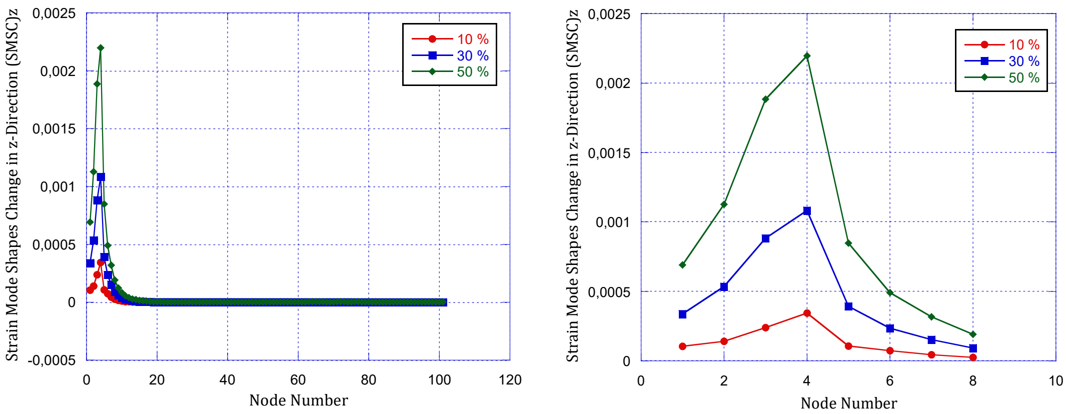

(a) **(b)**

Fig. 8 *Damage localization results by (SMSC) z for damage case 1. (a) (SMSC) $_z$ along the trailing edge; (b) Details around the damaged element*

Figure 9 illustrates the results of damage localization by the z-component of the SMSC for damage case 2. Damage case 2 consists of damaged element 3168, which is at the 84th and 85th nodes of the trailing edge. The z-component of the strain mode change presents a peak at the predetermined nodes of the damaged element for the different damage severity degrees, 10%, 30%, and 50%. The damaged element along the trailing edge can be accurately located by the z-component of strain mode changes for the various degrees of defect severity. However, the (SMSC) $_z$ at the neighbour element nodes of the defective element are also higher.

6.1.2 Strain Flexibility Change-Based Damage Indicator

The strain flexibility changes along the trailing edge are calculated by equation (10). Figure 10 shows the damage localization results by (SFC) $_z$ for defect case 1. It is observable that the (SFC) $_z$ indicator along the trailing edge presents a peak at the fourth node of the trailing edge. Therefore, the strain flexibility change in the z-direction pinpointed the damaged element. In damage case 2, Figure 11 illustrates the results of damage localization by the strain flexibility change. The SFC component in the *z*-direction pinpointed the position of the defective element. The values of strain flexibility change in the z-direction at the predetermined nodes of the defective element are higher than the values of (SFC) $_z$ at other positions. However, the (SFC) $_z$ at the neighbour element nodes of the defective element are also higher. Moreover, the values of (SFC) z at nodes of defective elements are lower than the values of (SMSC) z. The magnitude of (SFC) $_z$ at nodes of defective elements is proportional to the defect severity, as the defect severity increases as the magnitude of (SFC) z increases.

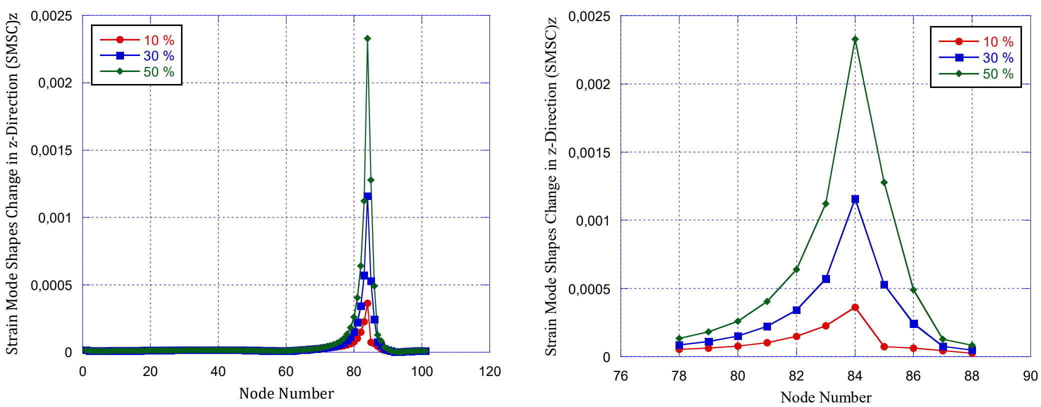

(a) **(b)**

Fig. 9 *Damage localization results by (SMSC) $_z$ for damage case 2. (a) (SMSC) $_z$ along the trailing edge; (b) Details around the damaged element*

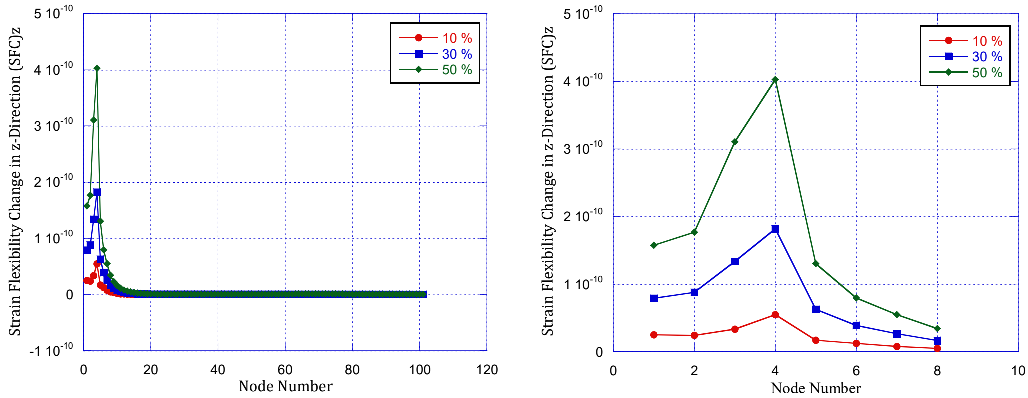

(a) **(b)**

Fig. 10 *Damage localization results by (SFC)* $_z$ *for damage case 1. (a)(SFC)* $_z$ *along the trailing edge; (b) Details around of damaged element*

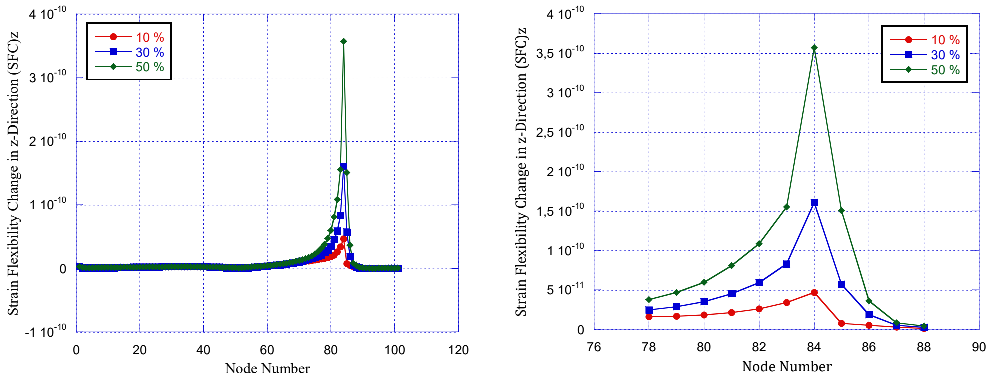

(a) **(b)**

Fig. 11 *Damage localization results by (SFC)* $_z$ *for damage case 2. (a)(SFC)* $_z$ *along the trailing edge; (b) Details around the damaged element*

It can be seen that the effect of damage on strain flexibility change is more important in the *z*-direction. It can be noted that the structural defect on the trailing edge of the marine propeller blade can be located and quantified accurately by the z-component of the strain flexibility change.

6.1.3 Defect Index

The z-component of the defect index along the trailing edge is calculated using equation (13). For damage case 1, the results of defect localization by the z-component of the defect index are illustrated in Fig. 12. It is observable that the component of the defect index in the *z*-direction reaches strictly positive values at the 3rd and 4th nodes on the trailing edge, which correspond to the predetermined nodes of the damaged element, and this observation is valid for the different degrees of defect gravity.

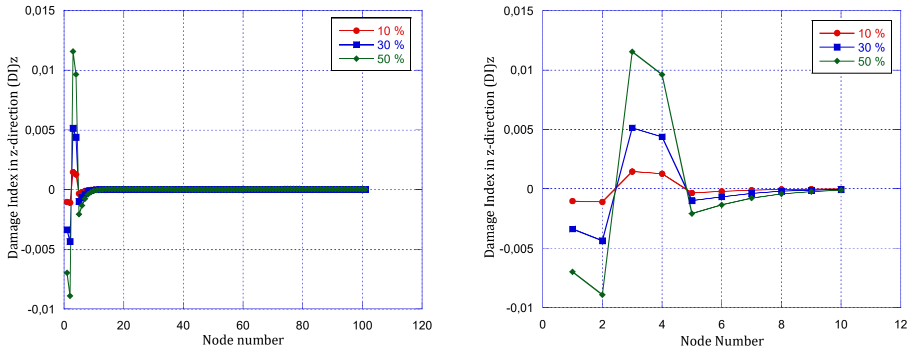

(a) **(b)**

Fig. 12 *Damage localization results by defect index in z-direction (DI) z for damage case 1. (a) (DI) z along the trailing edge; (b) Details around the damaged element*

Therefore, the component of the defect index in the z-direction successfully locates the damaged element near the root of the blade, and the identification quality is higher because the two predetermined nodes of the damaged element have been pinpointed. For damage case 2, the results of defect localization by the z-component of the defect index are illustrated in Fig. 13. It is observable that the component of the defect index in the *z*-direction reaches strictly positive values at the 84th and 85th nodes on the trailing edge.

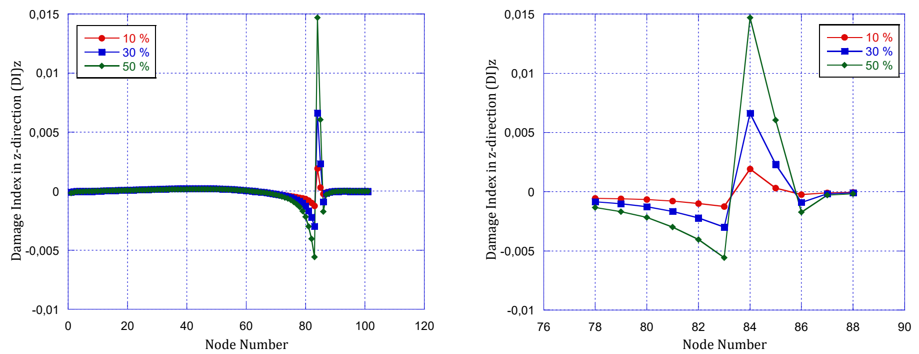

(a) **(b)**

Fig. 13 *Damage localization results by defect index in z-direction (DI) z for damage case 2. (a) (DI) z along the trailing edge; (b) Details around the damaged element*

The defect index values are higher only at nodes of the defective element; the values of the defect index at the neighbour element nodes of the defective element are lower. Moreover, the magnitude of (DI) z at the nodes of the defective element is higher than that of (SMSC) z, which allows a more precise localization of the defective element. Therefore, the damaged element is located successfully by this component of the damage index. For damage type on the trailing edge of the blade, it can be noted that the structural defect has a great effect in the *z*-direction, and the three proposed methods can successfully localize the defective element. The higher identification quality of the damaged element with different severity levels is obtained by using the defect index method.

6.2 Damage Localization on the Marine Propeller Blade Surface

In this section, two damage scenarios were considered (damage cases 3 and 4) to examine the capacity of the different strain defect indicators to locate the damaged element. The first specified damaged element is situated between the 3rd and the 4th node on the curve guide on the blade surface, and the second damaged element is at the 36th and 37th nodes on the curve guide.

6.2.1 Strain Mode Shape Change-based Damage Indicator

The SMSC in the *z*-direction was calculated along the curve guide of the blade using equation (7). Figure 14 illustrates the results of damage localization by the (SMSC) z for damage case 3. The component of *SMSC* in the *z*-

direction attains maximum values at the 3rd and the 4th nodes of the curve sensors for the varying levels of defect severity. The damaged element in the blade surface and near the blade root has been successfully localized by the $(SMSC)_z$. Figure 15 illustrates the results of defect localization by the $(SMSC)_z$ for defect case 4. It is observable that for the different degrees of defect gravity, the graph of the component of the *SMSC* in the *z* direction presents a not-sharp peak at the 36th and 37th nodes of the curve guide. The peak position corresponds exactly to the damaged element position. Therefore, the damaged element is successfully localized by the *z*-component of the SMSC indicator. The dynamic strain values at the marine propeller blade surface near the specified finite element (2092) are very high in the z-direction, so damage identification is easy. However, the magnitude of $(SMSC)_z$ at the neighbour elements' nodes of the defective element is relatively higher. Moreover, the magnitude of $(SMSC)_z$ at nodes of defective elements increases as the defect severity level increases. This relationship between the magnitude of (SMSC) z and defect severity level can be exploited for defect quantification.

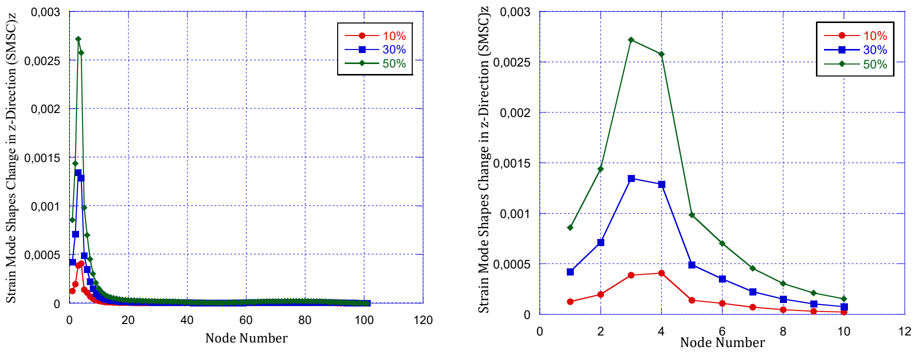

(a) **(b)**

Fig. 14 *Damage localization results by $(SMSC)_z$ on the blade surface for damage case 3. (a) $(SMSC)_z$ along the guide curve; (b) Details around the damaged element*

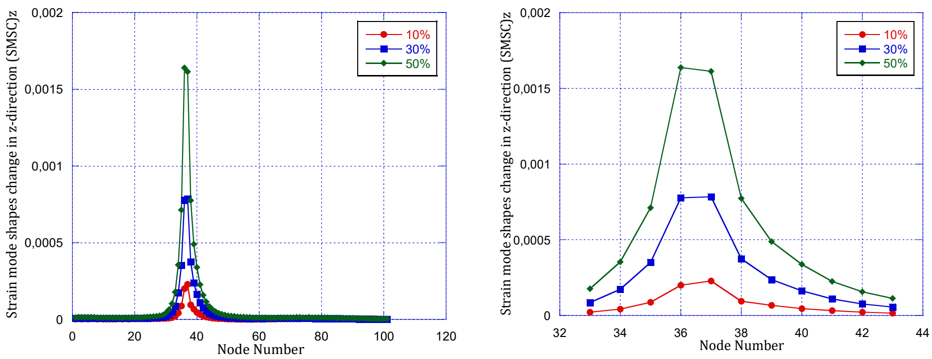

(a) **(b)**

Fig. 15 *Damage localization results by $(SMSC)_z$ on the blade surface for damage case 4. (a) $(SMSC)_z$ along the guide curve; (b) Details around the damaged element*

6.2.2 Strain Flexibility Change-Based Damage Indicator

The component in the z-direction of the strain flexibility change along the guide curve was calculated by Equation (10). The results of damage localization in the marine propeller blade surface for damage case 3 by the modal SFC are shown in Fig. 16. At the third and fourth nodes of the guide curve, which correspond to the nodes of the damaged element, the SFC in the z-direction exhibits a non-sharp peak. Thus, the SFC in the z-direction is more performant in locating the damaged element. The defect localization results by the SFC for defect case 4 are illustrated in Figure 17. It is observable that the strain flexibility change in the z-direction has the best performance in locating the damaged element because the two predetermined nodes of the damaged element have been localized. However, the values of $(SFC)_z$ at the neighbor elements' nodes of the defective element are also higher. Moreover, the magnitudes of $(SFC)_z$ at nodes of the defective element are lower than the values of $(SMSC)_z$ at the same nodes.

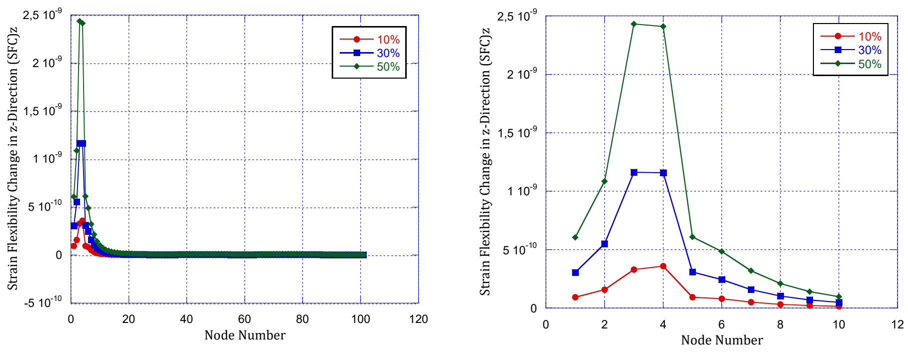

(a) **(b)**

Fig. 16 *Damage localization results by modal (SFC) z on the blade surface for damage case 3. (a) (SFC) z along the guide curve; (b) Details around the damaged element*

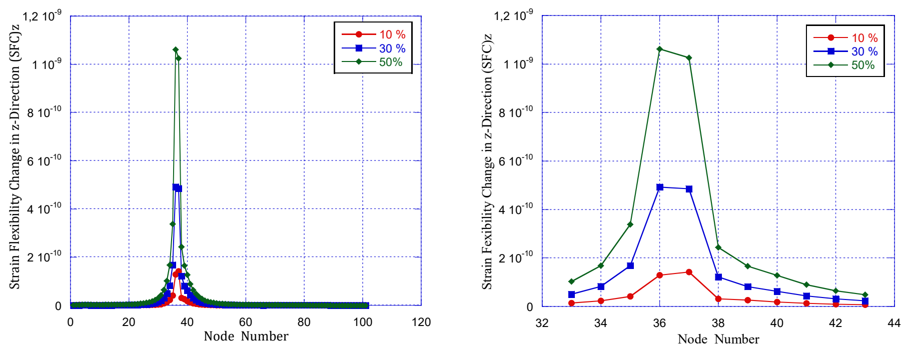

(a) **(b)**

Fig. 17 *Damage localization results by modal (SFC) z on blade surface for damage case 4. (a) (SFC) z along the guide curve; (b) Details around the damaged element*

6.2.3 Defect Index

The defect index in the z-direction is calculated by equation (13), and plotted along the guide curve. Figures 18 and 19 show the outcomes of damage localization on the blade surface by the damage index for damage cases 3 and 4, respectively. It is demonstrated that the defect index in the *z*-direction can locate the predetermined damaged element in the blade surface and for the different damage sizes. However, the damage index in the *z*-direction presents excellent results of damaged element localization, the values of $(DI)_z$ are higher only at the nodes of the defective element. The amplitude of $(DI)_z$ at the nodes of the defective element is higher than the amplitude of $(SMSC)_z$. For damage type on the blade surface, the damage index in the *z*-direction is a successful approach to locating the structural damage compared to the other modal strain-based damage identification methods. Moreover, the magnitude of the different defect indices at the nodes of the defective element is proportional to the defect severity level.

6.3 Multiple Damages Identification on the Leading Edge of the Marine Propeller Blade

In this section, three defect cases are considered to examine the ability of the different strain-based damage indicators to locate the multiple damaged elements along the leading edge of the propeller blade. To simulate multiple damage scenarios, four possible damaged element positions were chosen from the blade base to the free end of the blade. The first damaged element is situated between the 3rd and 4th nodes of the leading edge, the second is at (27-28) nodes, the third is between (45-46) nodes, and the latter is at (69-70) nodes of the leading edge. In case 5, only the first two damaged elements were considered. In damage case 6, the first three damaged elements were considered, and in the latter case, all four damaged elements were considered.

Int. Journal of Integrated Engineering Vol. 18 No. 3 (2026) p. 177-197

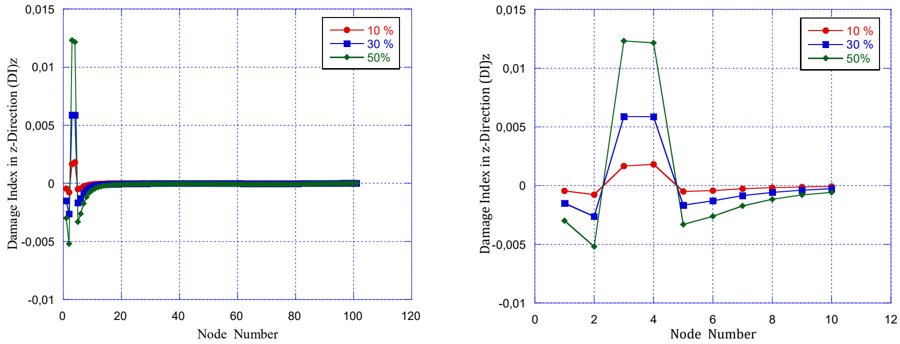

(a) **(b)**

Fig. 18 *Damage localization results by defect index (DI)* $_z$ *on the blade surface for defect case 3. (a)(DI)* $_z$ *along the guide curve; (b) Details around the damaged element*

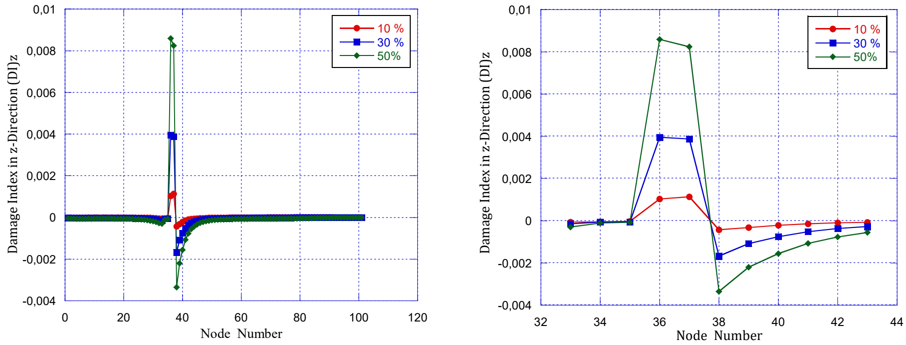

(a) **(b)**

Fig. 19 *Damage localization results by defect index (DI)* $_z$ *on the blade surface for defect case 4. (DI)* $_z$ *along the guide curve; (b) Details around the damaged element*

6.3.1 Strain Mode Shape Change-Based Damage Indicator

The modal strain change along the leading edge was calculated by equation (7). The results of multiple damage localizations by the (SMSC) $_z$ for damage case 5 are shown in Fig. 20. It is observable that the component (SMSC) $_z$ calculated with the mode shapes in the *z*-direction shows peaks at nodes of damaged elements and confirms the predetermined locations of the damage for the varying defect severities. Therefore, the component (SMSC) $_z$ successfully located the multiple damaged elements on the leading edge of the propeller blade. The result of SMSC to multiple damage localization for damage case 6 is shown in Fig. 21. In this case, three finite elements were considered simultaneously as damaged. The component in the *z*-direction shows no sharp peak, as the (SMSC) $_z$ values at the two nodes of the damaged element are very high. As a result, the component of the SMSC in the z-direction localizes the damaged elements with high accuracy. Figure 22 illustrates the results of multiple defect localizations by the (SMSC) $_z$ for defect case 7. As can be observed in the previous multiple damage cases, the z-component of SMSC can locate multiple defects up to four closely distributed on the propeller blade edge. Besides, the magnitudes of (SMSC) $_z$ at the nodes of the defective elements are proportional to defect severities. The amplitude of (SMSC) z at the node of the defective element increases as the defect position moves to the free end of the propeller blade.

6.3.2 Strain Flexibility Change-Based Damage Indicator

The component of strain flexibility change in the *z*-direction was calculated using equation (10).The results of multiple damage localizations by the (SFC) $_z$ for damage case 5 are shown in Fig. 23. The component of SFC in the *z*-direction shows two not-sharp peaks at the locations of the two defective elements and indicates with success both nodes of each damaged element.

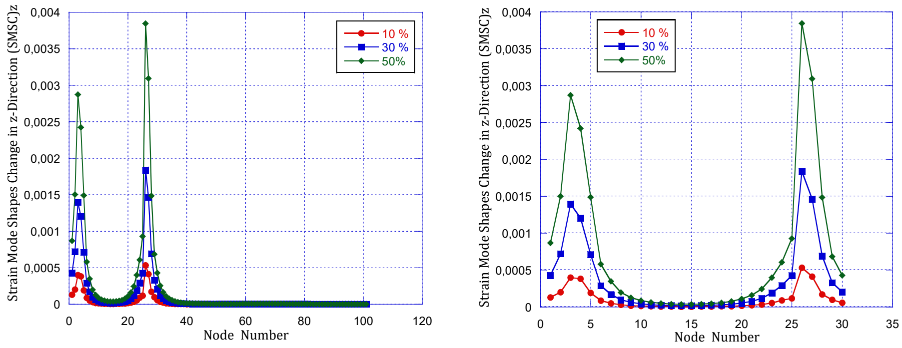

(a) **(b)**

Fig. 20 *Multiple damage localization results by (SMSC)* $_z$ *for damage case 5. (a) (SMSC)* $_z$ *along the leading edge; (b) Details around the damaged elements*

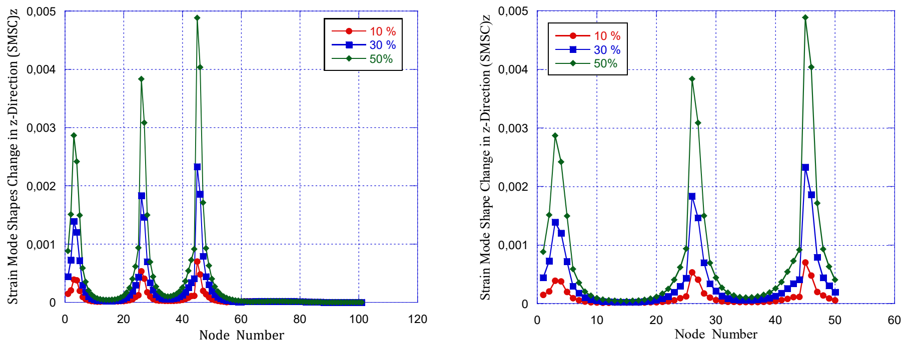

(a) **(b)**

Fig. 21 *Multiple damage localization results by (SMSC)* $_z$ *for damage case 6. (a) (SMSC)* $_z$ *along the leading edge; (b) Details around the damaged elements*

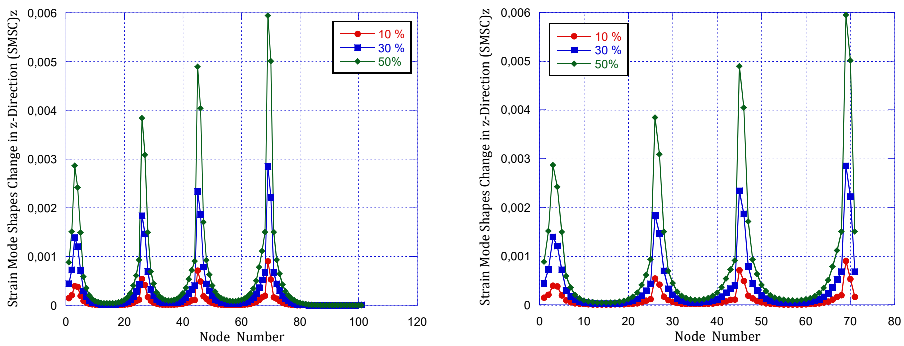

(a) **(b)**

Fig. 22 *Multiple defect localization results by (SMSC)* $_z$ *for defect case 7. (a) (SMSC)* $_z$ *along the leading edge; (b) Details around the damaged elements*

Figure 24 illustrates the results of multiple damage localization by strain flexibility change for damage case 6. As can be observed, the component in the *z*-direction of SFC can locate with high precision the three damaged elements. The results of defect identification by strain flexibility change for defect case 7 are shown in Fig. 25. In this case, four specified damaged elements are considered along the leading edge of the marine propeller blade. It can be observed that the component of strain flexibility change in the *z*-direction can locate the four damaged elements along the leading edge.

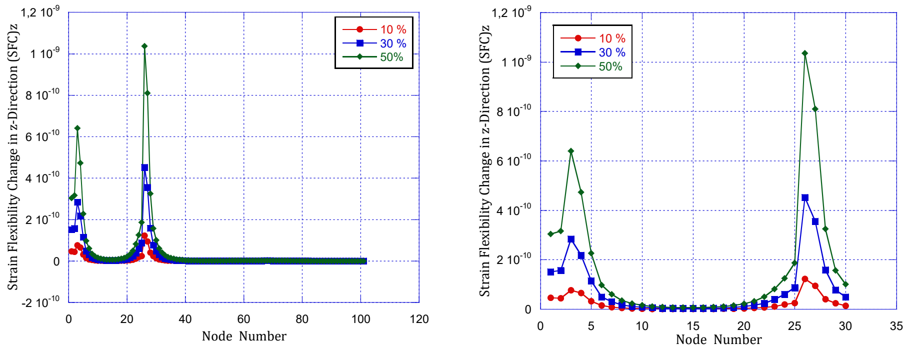

(a) **(b)**

Fig. 23 *Multiple damage localization results by (SFC)* $_z$ *for damage case 5. (a) (SFC)* $_z$ *along the leading edge; (b) Details around the damaged elements*

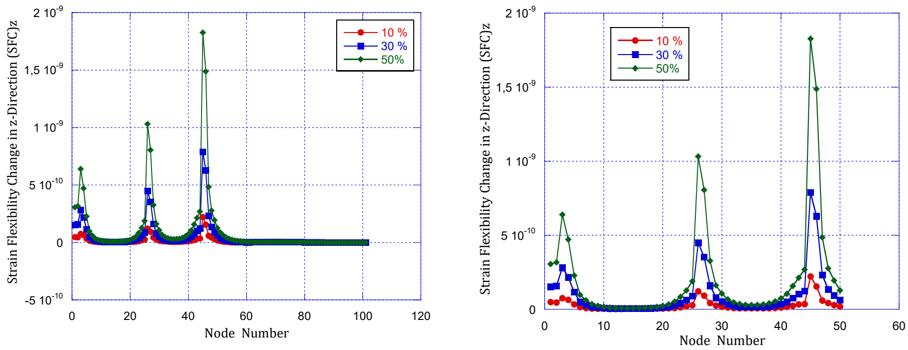

(a) **(b)**

Fig. 24 *Multiple damage localization results by (SFC)* $_z$ *for damage case 6. (a) (SFC)* $_z$ *along the leading edge; (b) Details around the damaged elements*

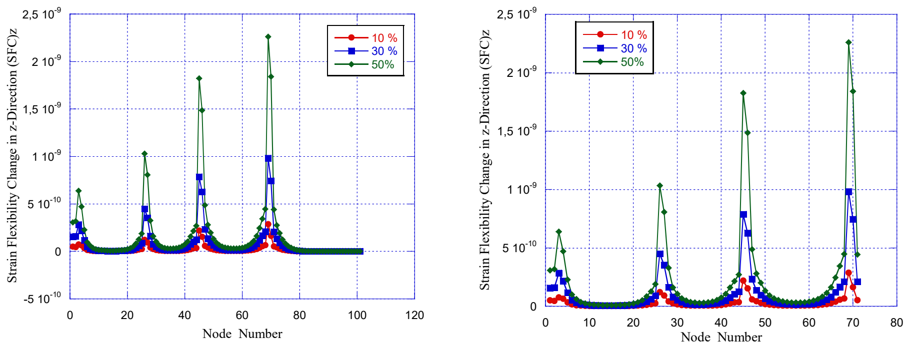

(a) **(b)**

Fig. 25 *Multiple damage localization results by (SFC)* $_z$ *for damage case 7. (a)(SFC)* $_z$ *along the leading edge; (b) Details around the damaged elements*

Moreover, the magnitude of (SFC) $_z$ at nodes of defective elements is proportional to defect severity at any defective element position. The magnitude of (SFC) $_z$ at the defect's position increases as the defect position moves to the blade tip. However, the amplitude of (SFC) z at the different defect positions is lower compared to that of (SMC) $_z$. The values of (SFC) z at neighbour elements' nodes of the defective elements are also higher, despite this, the (SFC) z can locate successfully multiple defects up to four simultaneously appeared and closely distributed along the propeller blade edge.

6.3.3 Defect Index

The component of the defect index in the z-direction along the leading edge is calculated using Equation (13). Figures (26)-(28) display the outcomes of multiple damage localizations on the blade's leading edge by the damage index for damage cases 5-7. Figure 26 displays the outcomes for damage case 5, which involves the incorporation of two damaged elements on the propeller blade's leading edge. The component of the damage index in the z-direction (see Figure 26) is capable of pinpointing the locations of the damaged elements with extreme precision and offers significant opportunities for damage assessment.

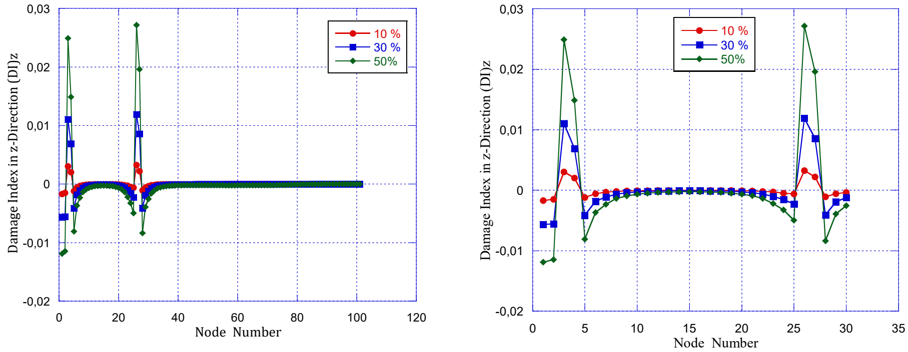

(a) **(b)**

Fig. 26 *Multiple damage localization results by damage index (DI) $_z$ for damage case 5. (a) (DI) $_z$ along the leading edge; (b) Details around the damaged elements*

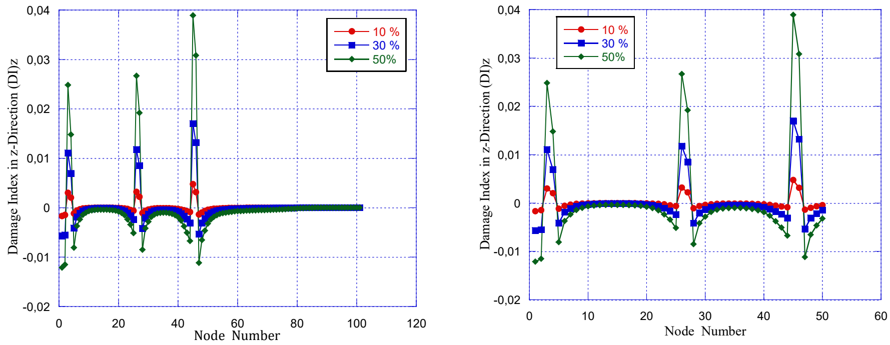

(a) **(b)**

Fig. 27 *Multiple damage localization results by damage index (DI) $_z$ for damage case 6. (a) (DI) $_z$ along the leading edge; (b) Details around the damaged elements*

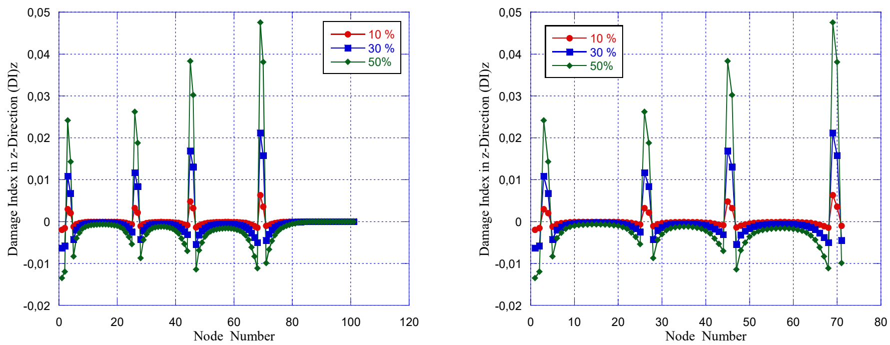

(a) **(b)**

Fig. 28 *Multiple damage localization results by damage index (DI) $_z$ for damage case 7. (a) (DI) $_z$ along the leading edge; (b) Details around the damaged elements*

Figure 27 displays the outcomes of multiple damage localizations by the damage index for damage case 6. The component of the damage index in the z-direction exhibits simultaneously three peaks along the leading edge at the predetermined locations of the three specified damaged elements. Figure 28 displays the multiple damage localization results by damage index for damage case 7. All damaged elements of varying degrees of severity can be successfully localized along the propeller blade's leading edge by using the component in the z-direction of the damage index. Moreover, the magnitude of the defect index $(DI)_z$ is higher only at the nodes of the defective elements, which allows a very precise localization of the defective elements, better than the two defect indicators, the $(SFC)_z$ and the $(SMSC)_z$, where their values are also high at the nodes of the elements neighbouring the defective elements. At the different locations of the defect, the magnitudes of the $(DI)_z$ are higher than the values of the $(SMSC)_z$ at the same locations. The defect index magnitudes at the nodes of the defective element increase as the defective element moves to the propeller blade tip. In addition, the magnitudes of the $(DI)_z$ at the nodes of all the defective elements are proportional to the severity of the defect; the magnitudes of $(DI)_z$ increase as the degree of the severity increases. If the leading edge of the blade sustains structural damage, then its major effect is in the z-direction, and higher identification quality of the multiple damaged elements with different severity levels is obtained by using the damage index method.

7. Conclusions

This article researches the location of single and multiple structural defects on the leading and trailing edges and the surface of marine propeller blades using vibration-based damage identification methods. Single and several defect scenarios have been modeled in the finite elements model of the marine propeller blade at different positions along the leading and trailing edges and on the blade surface. The strain modal analysis was executed in healthy and defective states of the marine propeller blade, and the first three strain mode shapes in the x, y, and z directions were calculated along the three lines according to the damage type. Dynamic strain-based damage identification techniques, such as strain mode shape change, strain flexibility change, and damage index, have been used for damage localization and assessment in the finite element model of the marine propeller blades.

Based on the numerical simulation results, it can be concluded that:

- The dynamic strain-based damage identification methods can accurately locate and assess single and multiple damages up to four of different sizes simultaneously appearing and closely distributed on the edges and surface of the marine propeller blade.
- The magnitude of DI at nodes of defective elements is higher (order of 10^{-2}) than the magnitude of SMSC (order of 10^{-3}), and much higher than the magnitude of SFC, which is of the order of 10^{-9}.
- The magnitudes of the three defect indicators, SMSC, SFC, and DI, at nodes of the defective element increase as the defective element moves to the marine propeller blade tip.
- The magnitude of the defect index (DI) is higher only at the nodes of the defective elements, which allows a very precise localization of the defective elements, better than the SMSC and SFC, where their magnitudes are also high at the nodes of the elements neighboring the defective elements.
- The magnitudes of SMSC, SFC, and DI at the nodes of the defective elements are proportional to the severity of the defects; the magnitudes of SMSC, SFC, and DI increase as the degree of the defect severity increases. Therefore, damage severity quantification on marine propeller blades based on the magnitude of damage indices at nodes of damaged elements is feasible.

The results obtained in this article can be used to monitor structural damage in propeller blades to extend their life spans.

Conflict of Interest

The authors declare that there is no conflict of interest regarding the publication of the paper.

Author Contribution

The authors confirm their contribution to the paper as follows: ***study conception and design:*** *Rachid Azzi, Farid Asma;* ***data collection:*** *Rachid Azzi;* ***analysis and interpretation of results:*** *Rachid Azzi, Farid Asma;* ***draft manuscript preparation:*** *Rachid Azzi, Farid Asma. All authors reviewed the results and approved the final version of the manuscript.*

References

[1] Jurkovič, M., Neslušan, M., Čep, R., Minárik, P., Trojan, K., Čapek, J., & Kalina, T. (2024). Magnetic non-destructive monitoring of a ship's propeller blade after long-term operation. Ocean Engineering, 291, 116470. https://doi.org/10.1016/j.oceaneng.2023.116470.

[2] Lee, C. S., Kim, Y. J., Kim, G. D., & Nho, I. S. (2002). Analysis of the structural failure of marine propeller blades. Journal of Ship and Ocean Technology, 6(3), 37-45. https://koreascience.kr/article/JAKO200211921502295.page.

[3] Pantazopoulos, G. A., Toulfatzis, A. I., & Tzompanakis, K. A. (2011). Failure Analysis of a Cast Mn-Bronze Propeller. Journal of Failure Analysis and Prevention, 11(3), 186-192. https://doi.org/10.1007/s11668-010-9428-6.

[4] Vizentin, G., Vukelic, G., Murawski, L., Recho, N., & Orovic, J. (2020). Marine propulsion system failures—A review. Journal of Marine Science and Engineering, 8(9), 662. https://doi.org/10.3390/jmse8090662.

[5] Yoon, H. Y., & Zhang, J. (2009). Prediction of fatigue life distribution of marine propeller materials. Journal of Mechanical Science and Technology, 23, 1323-1330. https://doi.org/10.1007/s12206-009-0112-2.

[6] Blednova, Z. M., Rusinov, P. O., & Dmitrenko, D. V. (2016). Failure analysis of screw propellers and increase of fail safety by surface modification with multicomponent materials with shape memory effect. Procedia Structural Integrity, 2, 1497-1505. https://doi.org/10.1016/j.prostr.2016.06.190.

[7] Li, Y. Y. (2010). Hypersensitivity of strain-based indicators for structural damage identification: A review. Mechanical Systems and Signal Processing, 24(3), 653-664. https://doi.org/10.1016/j.ymssp.2009.11.002.

[8] Wang, F., Li, R., Xiao, Y., Deng, Q., Li, X., & Song, X. (2021). A strain modal flexibility method to multiple slight damage localization combined with a data fusion technique. Measurement, 182, 109647. https://doi.org/10.1016/j.measurement.2021.109647.

[9] Philips Adewuyi, A., Wu, Z., & Kammrujaman Serker, N. H. M. (2009). Assessment of vibration-based damage identification methods using displacement and distributed strain measurements. Structural Health Monitoring, 8(6), 443-461. https://doi.org/10.1177/1475921709340964.

[10] HUANG, Z., XIONG, Y., & YANG, G. (2016). Composite propeller's strain modal and structural vibration performance. Chinese Journal of Ship Research, 11(2), 98-105. DOI: 10.3969/j.issn. 1673-3185.2016.02.013.

[11] Hong, Y., He, X. D., Wang, R. G., Li, Y. B., Zhang, J. Z., Zhang, H. M., & Gao, X. (2011). Dynamic responses of composite marine propeller in spatially wake. Polymers and Polymer Composites, 19(4-5), 405-412. https://doi.org/10.1177/0967391111019004-524.

[12] Javdani, S., Fabian, M., Carlton, J. S., Sun, T., & Grattan, K. T. (2015). Underwater free-vibration analysis of full-scale marine propeller using a fiber Bragg grating-based sensor system. IEEE Sensors Journal, 16(4), 946-953. https://doi.org/10.1109/JSEN.2015.2490478.

[13] Lin, H. J., & Tsai, J. F. (2008). Analysis of underwater free vibrations of a composite propeller blade. Journal of Reinforced Plastics and Composites, 27(5), 447-458. https://doi.org/10.1177/0731684407082539.

[14] Azzi, R., & Asma, F. (2024). Damage detection in marine propeller in service. Procedia Structural Integrity, 61, 241-251. https://doi.org/10.1016/j.prostr.2024.06.031.

[15] dos Santos, F. L. M., Peeters, B., Gielen, L., Desmet, W., & Góes, L. C. S. (2015). The use of fiber Bragg grating sensors for strain modal analysis. In Topics in Modal Analysis, Volume 10: Proceedings of the 33rd IMAC, A Conference and Exposition on Structural Dynamics, 2015 (pp. 93-101). Springer International Publishing. https://doi.org/10.1007/978-3-319-15251-6_11.

[16] Wang, Z., Sun, Y., Li, J., & Song, Z. (2024). Modal Parameter Identification and Damage Localization of Composite Helicopter Rotor Blades Based on AR/PR Identification. International Journal of Aerospace Engineering, 2024(1), 5716604. https://doi.org/10.1155/2024/5716604.

[17] Zhang, M., Valentin, D., Valero, C., Presas, A., Egusquiza, M., & Egusquiza, E. (2020). Experimental and numerical investigation on the influence of a large crack on the modal behaviour of a Kaplan turbine blade. Engineering Failure Analysis, 109, 104389. https://doi.org/10.1016/j.engfailanal.2020.104389.

[18] Wang, Y., Liang, M., & Xiang, J. (2014). Damage detection method for wind turbine blades based on dynamics analysis and mode shape difference curvature information. Mechanical Systems and Signal Processing, 48(1-2), 351-367. https://doi.org/10.1016/j.ymssp.2014.03.006.

[19] Rezaei, M. M., Behzad, M., Moradi, H., & Haddadpour, H. (2016). Modal-based damage identification for the nonlinear model of modern wind turbine blade. Renewable Energy, 94, 391-409. https://doi.org/10.1016/j.renene.2016.03.074.

[20] Tatsis, K., Ou, Y., Dertimanis, V. K., Spiridonakos, M. D., & Chatzi, E. N. (2021). Vibration-based monitoring of a small-scale wind turbine blade under varying climate and operational conditions. Part II: A numerical benchmark. Structural Control and Health Monitoring, 28(6), e2734. https://doi.org/10.1002/stc.2734.

[21] Wickramasinghe, W. R., Thambiratnam, D. P., Chan, T. H., & Nguyen, T. (2016). Vibration characteristics and damage detection in a suspension bridge. Journal of Sound and Vibration, 375, 254-274. https://doi.org/10.1016/j.jsv.2016.04.025.

[22] Wickramasinghe, W. R., Thambiratnam, D. P., & Chan, T. H. (2020). Damage detection in a suspension bridge using modal flexibility method. Engineering Failure Analysis, 107, 104194. https://doi.org/10.1016/j.engfailanal.2019.104194.

[23] Li, H., Yang, H., & Hu, S. L. J. (2006). Modal strain energy decomposition method for damage localization in 3D frame structures. Journal of Engineering Mechanics, 132(9), 941-951. https://doi.org/10.1061/(ASCE)0733-9399(2006)132:9(941).

[24] Epps, B.P.; Kimball, R.W.; (2013). OpenProp v3: Open-source software for the design and analysis of marine propellers and horizontal-axis turbines. URL: http://engineering.dartmouth.edu/epps/openprop.

[25] Zhou, Y., & Tao, J. (2019). Theoretical and numerical investigation of stress mode shapes in multi-axial random fatigue. Mechanical Systems and Signal Processing, 127, 499-512. https://doi.org/10.1016/j.ymssp.2019.03.015.

[26] Swamidas, A. S. J., & Chen, Y. (1995). Monitoring crack growth through change of modal parameters. Journal of Sound and Vibration, 186(2), 325-343. https://doi.org/10.1006/jsvi.1995.0452.

[27] Zonta, D., Lanaro, A., & Zanon, P. (2003). A strain-flexibility-based approach to damage location. Key Engineering Materials, 245, 87-96. https://doi.org/10.4028/www.scientific.net/KEM.245-246.87.

[28] Montazer, M., & Seyedpoor, S. M. (2014). A new flexibility-based damage index for damage detection of truss structures. Shock and Vibration, 2014(1), 460692. https://doi.org/10.1155/2014/460692.

[29] Stubbs, N., Kim, J. T., & Farrar, C. R. (1995, February). Field verification of a non-destructive damage localization and severity estimation algorithm. In Proceedings-SPIE the International Society for Optical Engineering (pp. 210-210). SPIE International Society for Optical.